



A 3D Free Surface Flow Modelling of Bypass Diversion Channel in Chao Phraya River using Large Eddy Simulation and Volume of Fluid Model

Chartchay Chumchan, Phadungsak Rattanadecho *

*Department of Mechanical Engineering, Faculty of Engineering,
Thammasat University, Pathum Thani 12120, Thailand*

Received 8 October 2019; Received in revised form 15 January 2020

Accepted 22 January 2020; Available online 24 December 2020

ABSTRACT

The aim of this work is to propose a fully free surface flow modelling technique to a feasibility study of flood prevention by using a bypass diversion channel. This work illustrates a case study in the area of west land of the Chao Phraya River in Ayutthaya City Island, Thailand. A full-scale geometry was created focusing on a simplified terrain model by using the SRTM3 dataset from the year 2000, which has a resolution of about 90 meters on the equator. The bypass diversion channel with 90° was constructed in the Chao Phraya River between Wat Tha Ka Rong and Wat Chaiwatthanaram. The numerical modelling is based on Large-eddy Simulation (LES) and Volume of Fluid (VOF) method that modelling in 3D was validated by using experimental data as partial dam-break flow, dam break in channels with 90° bend, and 90° lateral intake. The present study shows that the river flow in the main river flow can be reduced by using the bypass channel. Moreover, it is found that the formation of the separation zone in junction region that affect flood diversion, however, the length and size of the separation zone can be decreased by modifying the bypass junction shape.

Keywords: LES; VOF; Bypass channel; Dam-break flow; Flood diversion structures

1. Introduction

The 2011 flood event was one of the worst in Thailand in decades. The flood

caused many impacts in the Chao Phraya River basin region. A major research challenge is 3D numerical simulations of a

full-scale flood prevention feasibility study by using the example area such as Phra Nakhon Si Ayutthaya. This area is surrounded by three rivers, the Chao Phraya, Pasak, and Lop Buri; therefore, it is called Ayutthaya City Island or "Koh Mueng". Koh Mueng is an important archaeological site with residential areas and some minor commercial activities. This area was flooded because of the run-off of three rivers as the ground level is relatively low, resulting in a long inundation. The major flood protection of this area is a dyke over 5.30 m (Mean Sea Level, MSL). Despite this dyke, Koh Mueng was greatly affected during the severe flood in 2011. The lowest area is situated on the southwest side of Koh Mueng, which has an elevation of about 2.5 m (MSL), where the flood accumulates during flood events [1], see in Fig. 1.

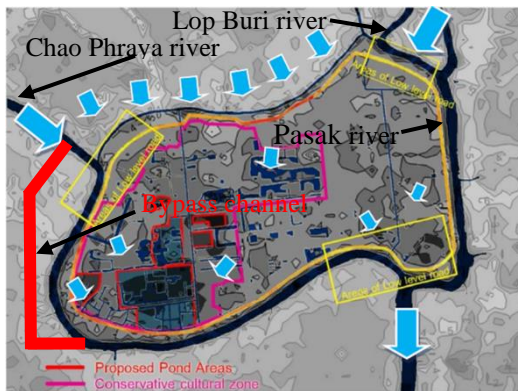


Fig. 1. Analysis of locations for potential flood mitigation measures and arrows indicate flood propagation towards the southwest region and bypass channel [1].

To prevent flooding in the Koh Mueng area, a flood diversion structure into which the flood can be diverted before flowing into the risk area is one solution. Fig. 1 shows bypass channels constructed in the Chao Phraya River between Wat Tha Ka Rong and Wat Chaiwatthanaram.

Many researchers proposed numerical models to understand the flow field in the open channel as well as some parameters that affect the performance of diversion

structures. Mah et al. [2,3] proposed an investigative modelling of the flood diversion structure in Kuching, Sarawak, by assessing its impact on the inundations of Kuching-Batu Kawa-Bau Expressway. In the past literature applied both 1D model based on the Saint-Venant equations, which has the advantage of simulating the flow scenarios in hours or days with low computing resources. Arega et al. [4] proposed a numerical model based on the general 2D shallow water equations to capture the discontinuity in hydraulic jumps of Yuen Long Bypass Floodway (YLBFB) at Hong Kong for optimum design arrangement of the bypass junction. However, due to supercritical-subcritical flow transitions, the complicated junction flow interactions (e.g., jet flows with eddies on both sides, hydraulic jumps) cannot be satisfactorily resolved by using 1D and 2D models. Free surface flow models in 3D need to be used to investigate secondary current and velocity distribution [5] that can dominantly control flow characteristics in a confluence region.

The flows analysis of open channel junction and confluence have been performed mainly with a strong focus on velocity information such as stagnation zone, the separation zone, the contracted flow region, and the shear layers [6–8], see in Fig. 2. The 3D flow patterns in junction and confluence are usually very turbulent and very complex states that the sizes of the separation zone affects to divert flows at the contracted flow zone.

To reduce the size of the separation zone in the open-channel junction, Firozjaei et al. [9] proposed a rectangular channel model without a slope to find the most suitable angle.

The numerical model was applied by simulating and considering the minimum size of the separation zone and Turbulent Kinetic Energy (TKE) in the bypass junction channel.

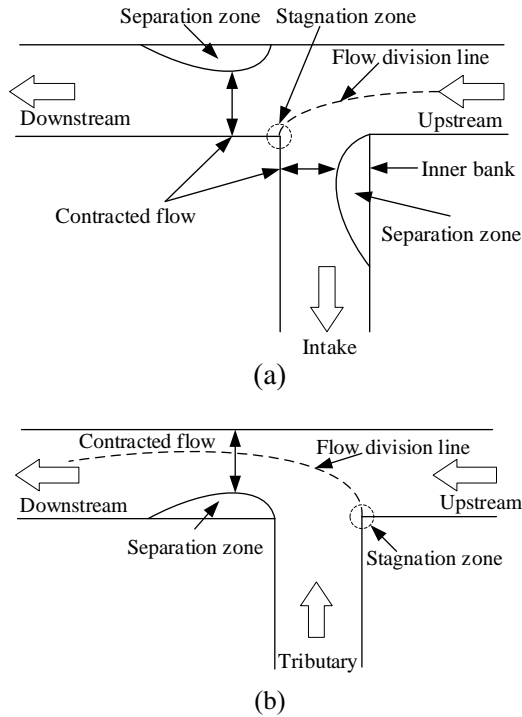


Fig. 2. (a) Flow pattern at 90° lateral intake (T-junction) and (b) flow characteristics at an open channel confluence.

After the operation in changing the water diversion angle at 30° , 45° , 60° , 75° , and 90° , it was concluded that 30° has the lowest values of turbulent kinetic energies, in which the minimum size of separation zones occurs in the side channel. However, natural rivers are often meandering and thus, design junctions and confluences should be optimized into specific shapes and the effects in open-channel junction such as junction angle, flow discharge, width ratios, and Froude number should be studied [10].

Due to high computational costs in 3D modelling of Direct Numerical Simulation (DNS), the Reynolds Averaged Navier Stokes equations (RANS) describe the transport of the averaged flow quantities, with the entire range of the scales of turbulence being modelled resulting in a significant reduction in computational cost. However, the RANS approach, for example the $k-\epsilon$ model, has limitations involving turbulence closures. Therefore, to simulate

near-field and turbulent behaviour, the Large-eddy simulation (LES) model can be actually captured such as surface-velocity fields, water level, bottom pressure and velocity variation with time [11]. For the LES model, the Navier–Stokes equations (NS-equations) are filtered, and large-scale eddies are resolved directly, while small eddies are modelled by Sub Grid Scale (SGS) [12].

Generally, the NS-equations can be discretized by using different numerical schemes (e.g., Finite-difference (FD), finite-element (FE), and Finite-volume (FV)), for which the computational domain is represented by using cells. Traditional mesh generation methods include the use of boundary-fitted curvilinear coordinate systems and unstructured grids with an irregularly shaped mesh. The unstructured grid is able to handle complex geometries more easily than a structured grid and ease local refinement grids. Suiju et al. proposed a numerical model to simulate the continuous bends of the Yellow River in the Shapotou section by using an unstructured-grid and the SIMPLE algorithm. These results show that the proposed model can accurately simulate the flow of 3D curves of natural rivers with complex boundaries [13]. In the case of shallow water flow, Kim et al. [14] used Cartesian cut-cell method to simulate dam-break flow propagation. The Cartesian cut-cell method can represent a complex domain accurately with less computational efforts [15–17] and the numerical results show good agreement with available laboratory measurements. Also, polyhedral cells have the potential to deliver more accurate results under certain flow conditions than hexahedral cell types [18]. Wang et al. [19] compared the performance of different meshes among polyhedral, tetrahedral and hexahedral in urban flood simulation. This study found that the polyhedral mesh was less dependent on grid number, used less computing time and had better convergence compared with the tetrahedral grid. For the

high Reynolds numbers flow, Garimella and Shephard [20] proposed boundary layer meshing for viscous flows in complex domains with meshes layer. In addition, the cells can be embedded in geometric features by defining the fraction face areas and fraction volume of the rectangular cells, the so-called Fractional Area-Volume Obstacle Representation (FAVOR) technique mesh method that was developed and implemented into the FLOW-3D software [21,22]. In recent years, Smoothed Particle Hydrodynamics (SPH) and the Lattice Boltzmann Method (LBM) approaches have been proposed to reduce the preparation time for the meshing process. The SPH approach was developed to solve NV-equations in the Lagrangian setting of notional fluid particles. Alternatively, instead of solving the NV-equations, the LBM model was inspired by the kinetic theory of gases that the Boltzmann transport equation solved and modeled gas behavior at the mesoscopic scale [23]. As the meshing process is avoided, SPH and LBM methods have become popular for high-Re and multiphase flows [24–27].

For free surface flow model, many techniques are applied to track the air-water interface. Volume of Fluid (VOF) is one of the best-known capture methods [28–31] in which the tracking of the interface is accomplished by calculating a continuity equation. Munoz and Constantinescu [32] proposed the 3D modelling of RANS-VOF model to simulate flooding events in the Iowa River near Iowa City, Iowa, USA. Recently, the VOF approach has combined both FVM and LBM models that have been widely used in many commercial CFD software programs (e.g. Flow-3D, CFX, Fluent, OpenFOAM, Star CD, XFlow, etc.).

Therefore, this work uses the LES model combination with VOF method to simulate the unsteady free surface flow in 3D when the bypass diversion channel is constructed in an interesting area. The computational domains were obtained from a

full-scale terrain of Digital Elevation Model (DEM) data, which is available free of cost at <http://jthatch.com/Terrain2STL/>. The DEM data was modified by adding different sizes of bypass channels to be more realistic for this study. The grids were generated by using a Cartesian cut-cell grid method with boundary layer mesh and local cell refinement. The water level and velocity contour in the river were studied and compared.

2. Governing Equations

In this work, the LES and VOF models are used to track the flow patterns of free surface flow. In the CFD code, the filtered equations, which express conservation of mass and momentum for an incompressible flow, can be written by using the conservative form [33],

$$\frac{\partial \alpha_q \bar{u}_i}{\partial x_i} = 0, \tag{1}$$

$$\frac{\partial (\rho \bar{u}_i)}{\partial t} + \frac{\partial (\rho \bar{u}_i \bar{u}_j)}{\partial x_j} = \tag{2}$$

$$-\frac{\partial \bar{p}}{\partial x_i} + \mu \frac{\partial \bar{u}_i}{\partial x_j \partial x_j} + \rho g_i + \frac{\partial \tau_{ij}^r}{\partial x_j} + F_i^{vol},$$

where \bar{u}_i is the filtered resolved quantity in the i direction and x_i is the i -coordinate in the Cartesian coordinate system; \bar{p} represents the filtered pressure, and τ_{ij}^r is the residual stress tensor ($i, j = 1, 2, 3$). where p is pressure (kPa), g_i is gravitational acceleration, F_i^{vol} is i -component of volume force.

In the calculation, Navier–Stokes equations are filtered, and large-scale eddies are resolved directly, while small eddies are modeled by sub-grid scale (SGS) modelling with Smagorinsky model [34]:

$$\tau_{ij}^r = -2\nu_t \bar{S}_{ij}, \tag{3}$$

where \bar{S}_{ij} is the rate of strain tensor for the

resolved scale defined by;

$$\bar{S}_{ij} = \frac{1}{2} \left(\frac{\partial \bar{u}_i}{\partial x_j} + \frac{\partial \bar{u}_j}{\partial x_i} \right), \quad (4)$$

and ν_t is the sub grid eddy viscosity given by:

$$\nu_t = l_s^2 S = (C_s \Delta)^2 S, \quad (5)$$

where l_s is the mixing length of sub-grid scales, C_s is Smagorinsky coefficient, Δ is computed according to the volume of the local computational cell, and S is the strain-rate tensor given by $\sqrt{2} |S_{ij}|$. Note that $C_s = 0.1$ is given as a default value in ANSYS-Fluent.

The VOF model proposed for tracking the gas-liquid interface is achieved by solving the continuity equation for the volume fraction (α) of the two fluid phases. Hence for the q^{th} phase, the continuity equation has the following form:

$$\frac{\partial \alpha_q \rho_q}{\partial t} + \frac{\partial}{\partial x_j} (\alpha_q \rho_q u_j) = 0, \quad (6)$$

where u_j is velocity. By knowing the constant density ρ and the viscosity μ of fluid, Eq.6 can be reduced to

$$\frac{\partial}{\partial x_j} (\alpha_q u_j) = 0. \quad (7)$$

The volume fraction equation is solved only with the secondary liquid phase, while the phase fraction of the primary gas is calculated as follows:

$$\sum_{q=1}^n \alpha_q = 1. \quad (8)$$

The momentum equation is given by:

$$\rho \left(\frac{\partial u_i}{\partial t} + u_i \frac{\partial u_i}{\partial x_j} \right) = - \frac{\partial p}{\partial x_i} + \mu \frac{\partial u_i}{\partial x_j \partial x_j} + \rho g_i + F_i^{vol}, \quad (9)$$

The Continuum Surface Force (CSF) model [35,36] is used to simulate surface tension of fluid. The surface force per unit volume is computed only within each surface cell and is placed at the center of the cell:

$$F_{i,j,k}^{vol} = \sigma \kappa_{i,j,k} \frac{A_{i,j,k}}{V_{i,j,k}} n_{i,j,k}, \quad (10)$$

where σ is the surface tension coefficient, $\kappa_{i,j,k}$ is the local surface curvature defined by the divergence of the unit normal, $A_{i,j,k}$ is the surface area of the interface within the cell, $n_{i,j,k}$ is unit vector normal to the surface, and $V_{i,j,k}$ is the volume of the cell denoted by i,j,k .

The default properties of air and water are adopted in ANSYS Fluent commercial software. The density of water is equal to 998.2 kg/m³, and that of air is equal to 1.225 kg/m³. The surface tension coefficient is equal to 0.072 N/m.

When the boundary layer of the viscous flow region is important, the vicinity at wall boundary conditions requires special treatment. The universal rule of the so-called wall describes the flow profile in flow regime. This can be done by determining the dimensionless velocity (u) and the distance from the wall (d) as a function of the shear velocity (u_τ) and viscosity (ν) [37]

$$y^+ = d \frac{u_\tau}{\nu}. \quad (11)$$

The schematic velocity profile near the wall in a turbulent boundary layer subdivides boundary layers into three zones according to the shape of their velocity profile: the viscous sub-layer ($y^+ < 5$) is characterized by a linear correlation between $u^+ = u/u_\tau$ and y^+ , the

buffer sub-layer ($5 < y^+ < 70$) is observable as turbulent and laminar features coexist, and the logarithmic sublayer ($y^+ > 70$) is characterized by fully developed flow profile in the turbulence region.

It is known that large gradients of property occur in the lowest y^+ regions. For this reason, wall functions can be implemented in CFD codes to model these regions instead of directly solving them. This allows the use of coarser mesh thus saving significant amounts of computational resources. These functions assume that the behavior of viscous sub-layers is universal. Therefore, their main requirement is those mesh elements in contact with solid boundaries must have y^+ values between the buffer and the logarithmic sub-layers ($y^+ \sim 35$).

The time step Δt is determined according to the Courant-Friedrichs-Lewy (CFL) condition as Eq.12 [33].

$$\Delta t = \frac{V_{cell,min}^{1/3}}{U}, \quad (12)$$

where U is the free-stream velocity (m/s) at inlet and $V_{cell,min}$ is the minimum volume of the computational domain.

To obtain the convergence results for numerical models of in this work, the terms discretizing scheme is used in the PISO algorithm (Pressure-Implicit with Splitting of Operators) for splitting the relationship is pressure- velocity coupling. The spatial discretization of the convection used least squares cell-based. The variable pressure was discretized with the PRESTO! (PREssure STaggering Option) scheme, and momentum was solved by the Quadratic Upstream Interpolation for Convective Kinematics (QUICK) scheme. Next, the compressive discretization scheme was applied with the implicit scheme for VOF based models. The transient formulation is bounded second-order implicit for setting different time-

dependent solution formulations. The computer configurations in this work were conducted by using dual processors of Intel Xeon E5-2660v2 and 32 GB of ECC- RAM.

3. Validation Model

To validate the numerical models of unsteady flow in 3D modelling, the static pressure and velocity in case of the partial dam-break flow [28] were investigated by using different turbulence models and validating with experimental data. Then, the precise numerical model in the previous case was chosen to investigate the free surface level of dam-break flow in a channel with 90° bend [38]. Furthermore, to study the flow pattern of the junction channel, the velocity profiles in the 90° lateral intakes channel was simulated and validated by experimental data [8,39].

3.1 Dam-break flow caused by partial failure

The configuration of partial dam-break model conducted by 3 m long, 2 m wide, and 0.7 m high flume, as shown in Fig. 3. The dam was represented by using two impervious vertical walls and a 0.4 m wide gate located between the walls at 1 m from the upstream end of the flume. The initial water depth (h_0) in the reservoir was 0.6 m. The downstream channel bed was dry and the pressure- outlet boundary condition was applied into top, side, and end of the domain. The dam-break incidence was represented by opening the gate immediately. The static pressure and velocity were predicted at different points as see in Fig. 4. Gauge points at G-5A, G-3A, and G-2A were placed inside the reservoir, G0 at the dam site, and G-2A downstream of the dam. The dam-break flow was the free-surface problem that is modelled by VOF based models for all turbulence models. The different turbulence models include LES (FVM), Renormalization Group (RNG), and LBM.

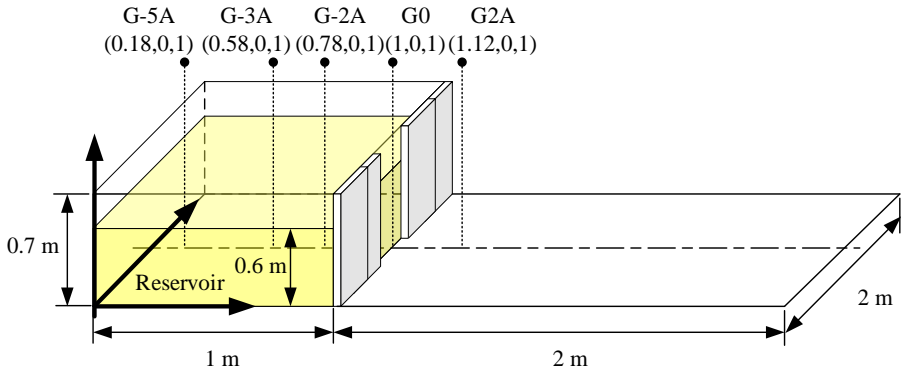


Fig. 3. Sketch of the partial dam-break experiment.

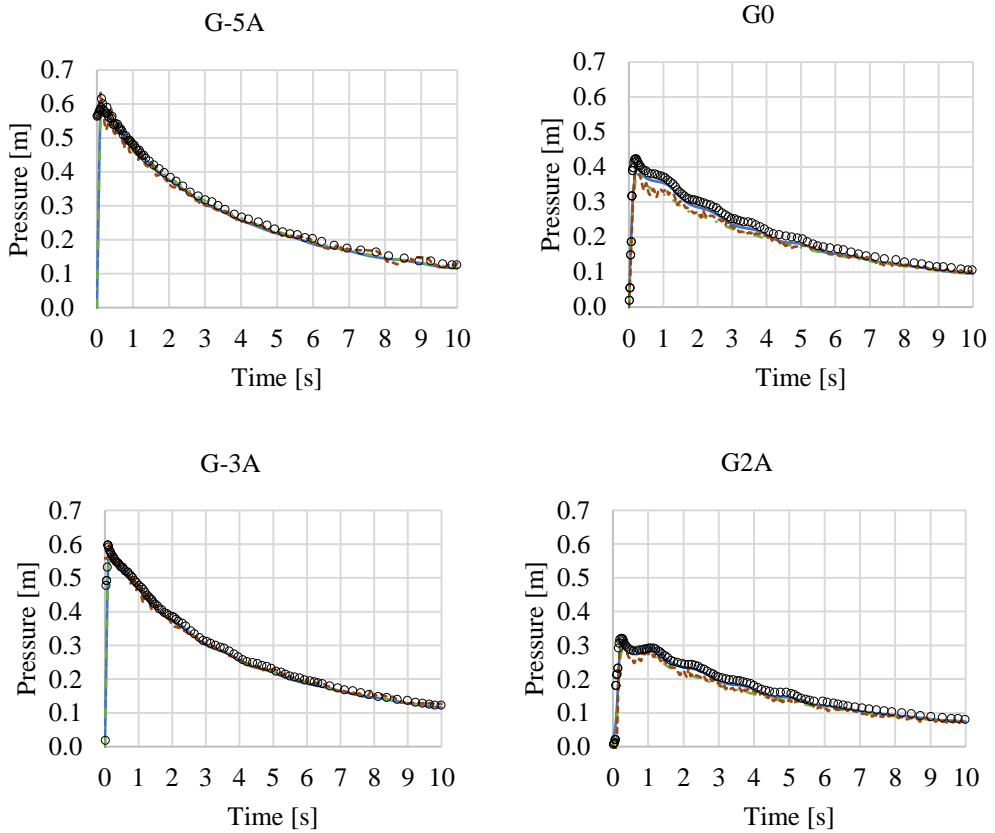


Fig. 4. Comparison of experiment and simulation pressure in the longitudinal direction at different vertical distances: ° EXP. — LES - - - RNG - - - LBM.

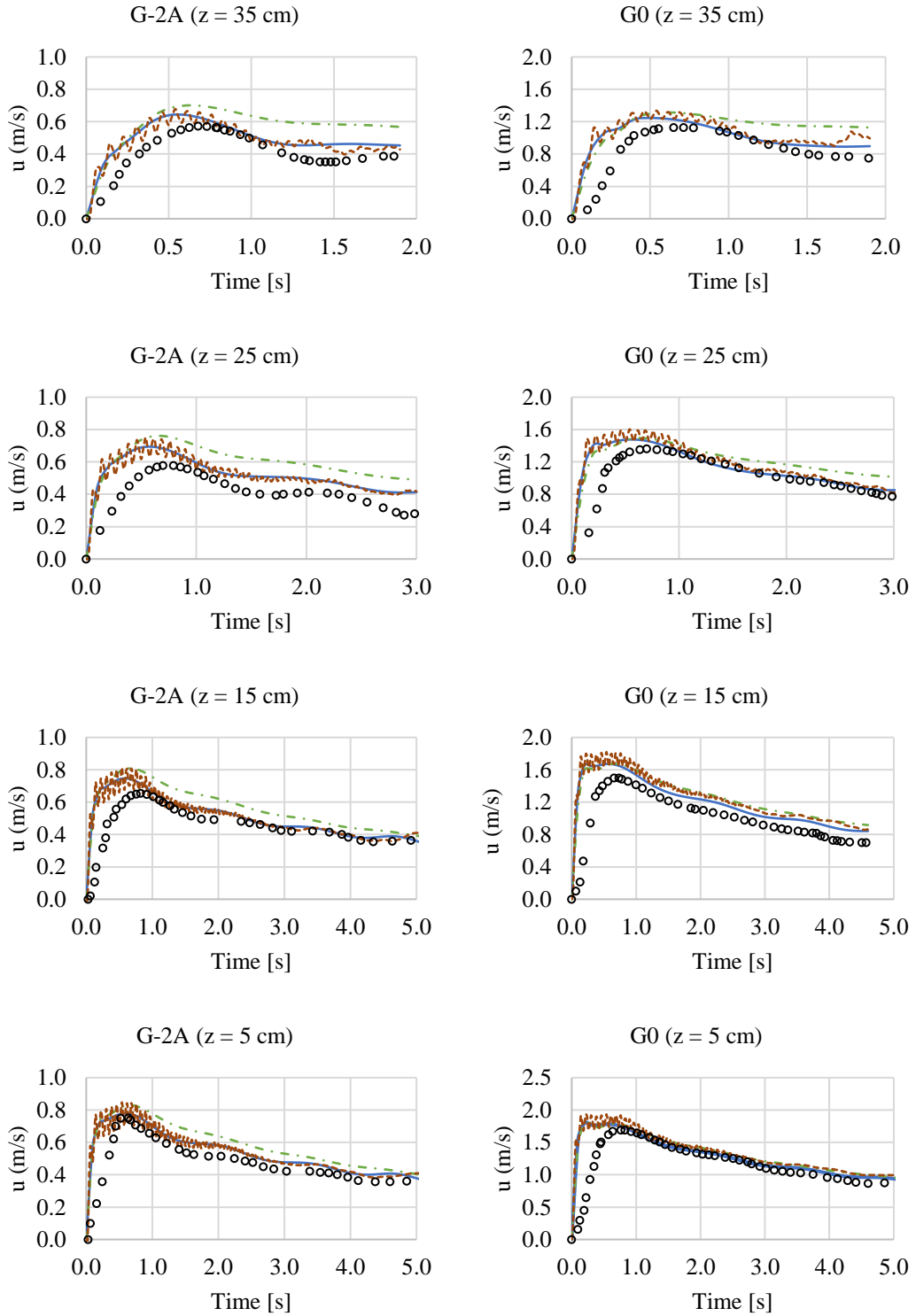


Fig. 5. Comparison of experiment and simulation velocities in the longitudinal direction at different vertical distances from the bed: \circ EXP. — LES - - - RNG - - - LBM.

The FVM grid was generated by using the Cartesian cut-cell grid method with grid spacing of 0.02 m, with the total grid equal to 519,400 cells. The time step size of unsteady flow process was calculated by estimating the maximum possible velocity of the interface (air- water) and the grid cell dimension as $U = \sqrt{2gh} = 3.431$ m/s. When using $C = 1$, the time step was 0.005 s. For the physical time of flow 10 s, 1,000 time steps were applied. The maximum iteration per time step was 50. Furthermore, the total cubic lattices grid of LBM model was 504,560 elements.

Fig. 4 shows a comparison of static pressure at different gauge points of G-5A, G-3A, G2A, and G0 with experimental data. It was found that the LES model was more accurate than the other cases. Fig. 5 shows validation results with experimental data of the longitudinal flow velocity in different levels above the bed consist of 0.05 m, 0.15m, 0.25 m, and 0.35 m at gauge points G- 2 A and G0. The comparison shows a temporal gap in which the predicted velocity reaches the peak value of about 0.3 s before the measure one. This might be due to the

rotational motion of the gate removal process in the experiment, whereas the model assumes sudden removal. After reaching the maximum value, the experimental and numerical velocity decreased with similar behavior. However, the FVM-LES model can capture the velocity better than other cases. Furthermore, the magnitude results of the LBM model were high oscillations then more error when the water became shallower.

3.2 Effects of a sharp 90° bend on dam-break flow

The experimental test-set was carried out in the Civil Engineering Laboratory of the Université Catholique de Louvain (UCL, Belgium). According to Fig.6, the test-set is built in such a way that it can be separated into two parts, which allows changing the straight shape by inserting channel bend with 90° element between the upstream and downstream reaches. The downstream channel was conducted by using a rectangular cross-section of 0.495 m width × 0.25 height and 7.6 m long.

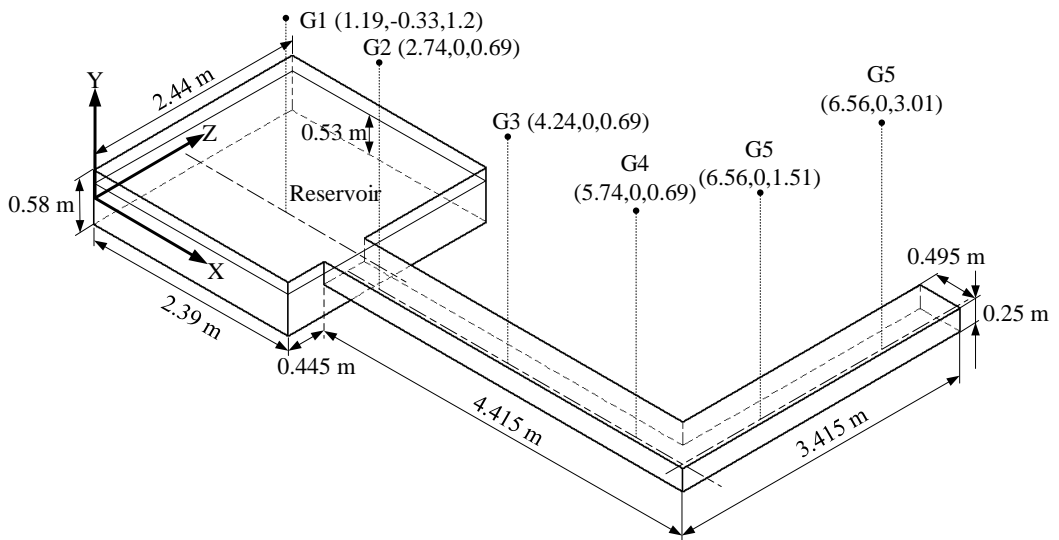


Fig. 6. Dam break flow with a sharp 90° bend - origin of the XYZ axes in the lower left corner (dimensions in m).

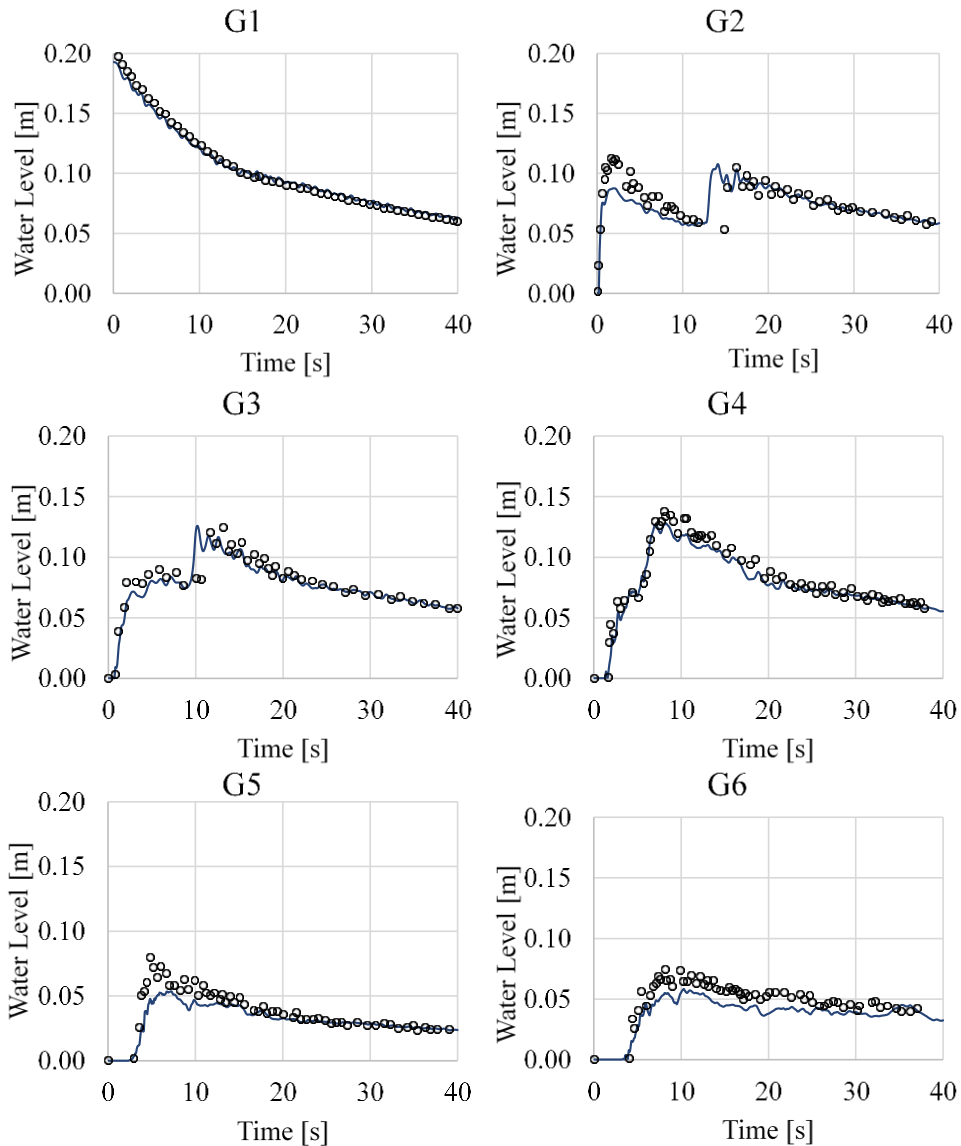


Fig. 7. Comparison of experiment and simulations of water level in the G1, G2, G3, G4, G5 and G6 with respect to time: ° EXP. —LES.

The reservoir has dimensions of 2.44 m × 2.39 m and the dam-break incidence was represented by a lift gate as instantaneous. The reservoir bottom level is 0.33 m lower than the origin, which means that there is a step at the entrance of the upstream channel. The initial water level in the upstream reservoir (h_0) is 0.20 m above the origin level. The experiment data were carried out by using different six-gauge points. The numerical

model was applied by using LES with Smagorinsky model and VOF model.

The computational grid was generated by a Cartesian cut-cell grid with an equal grid spacing of 0.02 m that grids was 558,475. The time step size was calculated by estimating the maximum possible velocity of the interface and the grid cell dimension as $U = \sqrt{2gh} = 1.981$ m/s and using $C = 1$, time step was equal to 0.005 s. The number of

time steps was 8,000 for the physical time 40 s. Moreover, the maximum iterations per time step was 50.

According to Fig. 7 the comparison result shows that between water level and arrival time. Point G1 shows the validation results in the upstream reservoir that decrease during 0- 40 s. It was found that the draining curves match closely. From points G2 to G6, the simulation results tend to be close to experimental data so that the hydraulic jump can be predicted when a wave front impacted the channel bend.

3.3 Flow pattern at 90° lateral intake

To study flow pattern in the bypass junction channel, the 90° lateral intake model was simulated and modelled by using only the LES model with Smagorinsky (SGS) model. Then the velocity profiles were validated by using experimental data. The laboratory specifications used in this case are the rectangular channel structure. The model was developed and empirically tested by Barkdoll et al [8] that data graph gave from publication paper [39].

According to Fig. 8(a) the main channel length is 2.74 m and the side channel length is 1.68 m. The side-channel in this experiment is located at 1 m from the main entrance. The channel width (b) is equal to 0.152 m. The prediction cross-section at x - and z - axes is defined by X^* and Z^* ratio, which X^* and Z^* are distance ratio from origin of x - and z - direction to channel width (b), respectively.

The total discharging was determined by $0.011 \text{ m}^3/\text{s}$ and a constant depth $h_0 = 0.31 \text{ m}$. The average velocity in the inlet is equal to 0.234 m/s . The boundary conditions of main-channel and side-channel outlets were considered by using pressure-outlet. The side and bottom surfaces were considered as the no-slip wall boundary conditions. The fluctuations of waves on the water surface are not considered since the symmetry boundary condition was applied on the top

surface domain. The grid-independent test for the size was carried out which ultimately led to the choice of the grid with $135 \times 35 \times 35$ cells in the main-channel and $50 \times 35 \times 35$ cells in the side-channel (226,625 elements), as seen in Fig.8(b). Besides, the dimensionless wall distance in mesh for boundary layer was calculated by using $y^+ < 5$ and Reynolds number (Re) 72,368 so that the first height was about $< 0.001 \text{ m}$ above the bottom wall. Next, the time step size (0.01 s) and the number of time steps (10,000) were chosen for the flow time 100 s. Also, the maximum iteration per time step was 20.

The results show that the dimensionless velocity profiles (U/U_{max}) versus dimensionless of channel width at discharge ratio (Q_r) is equal to 0.31, which Q_r is flow rate ratio of side-channel to main-channel. U_{max} is the maximum velocity at the cross-section $X^* = -4.15$ that U_{max} was about 0.28 m/s . Fig. 9 and Fig. 10 show that the comparison results found close tendencies. At the distance ratio of $X^* = -4.15$ (before junction region), the upstream velocity profile indicates the fully developed flow. The distance ratio of $X^* = 0$ shows the maximum velocity when flowing close to the entrance of side-channel. The velocity profiles at $X^* = 1$ and $X^* = 2$ show the lower velocity at downstream when flowing past the junction region. According to Fig.10, the distance of $Z^* = 1, 1.1, 2, 3,$ and 4 indicated flow behavior as diversion water entered the side channel. Due to the pressure moving away from the inner wall ($X^* = 0$) the velocity at the contracted flow zone (right side of side-channel) was higher than the entrance region because flow was squeezed by increasing the dimension of the separation zone. The simulation results in Fig. 11 show the velocity contours of different discharge ratios 0.25, 0.31, and 0.64, respectively. The increasing of the discharge ratio caused a decrease in the separation zone dimension in the side-channel.

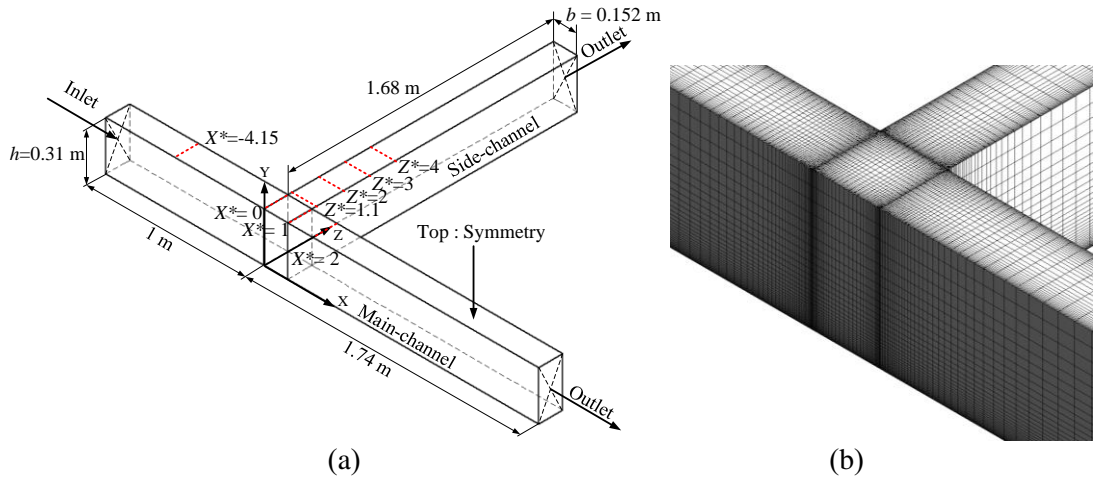


Fig. 8. Computational domain of 90° lateral intake: a) Geometric and boundary conditions, b) the computational grid.

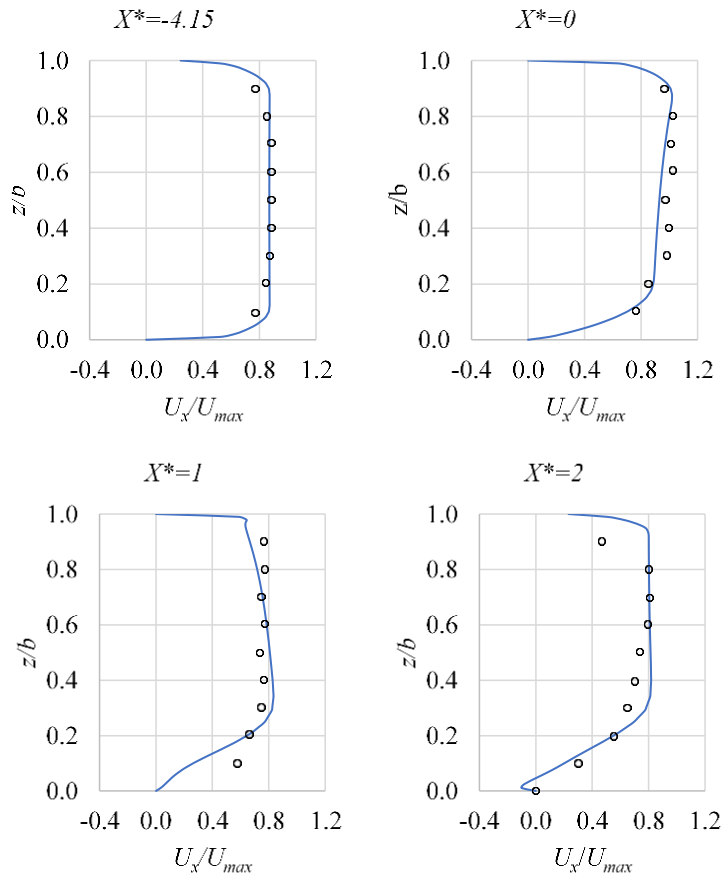


Fig. 9. Comparison of velocity profiles at different sections of the main channel: ° EXP. — LES.

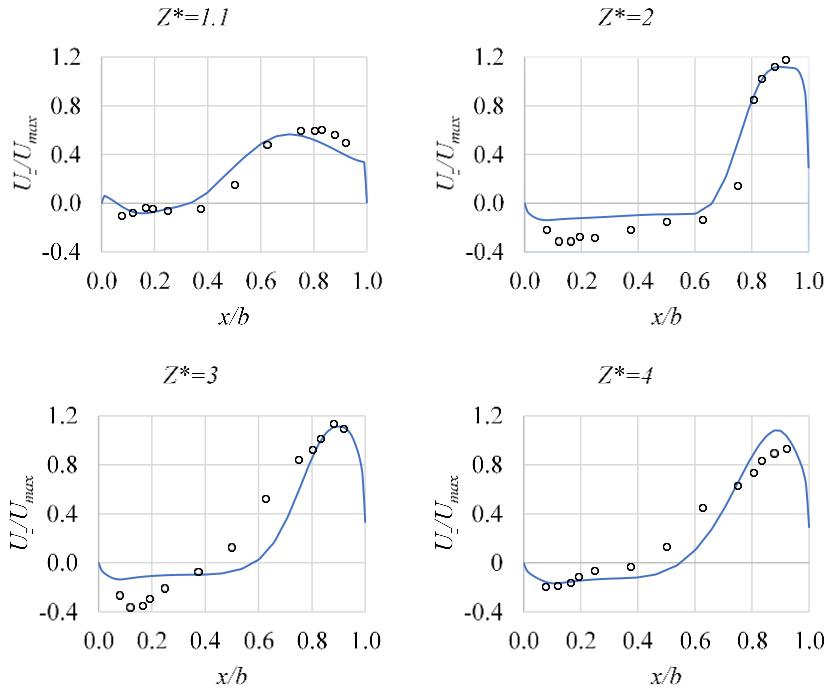


Fig. 10. Comparison of velocity profiles at different sections of the intake channel: ° EXP. — LES.

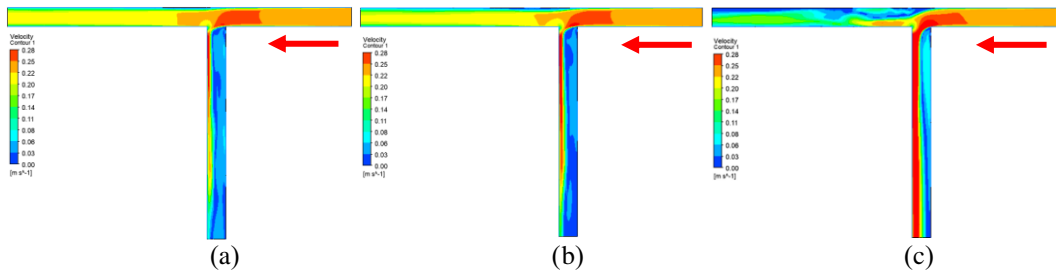


Fig. 11. Flow contour on the plane close to water surface comparison at different discharge ratio as a) $Q_r = 0.25$, b) $Q_r = 0.31$, and c) $Q_r = 0.64$.

Additionally, the high discharge ratio effected separation zone formation in main channel downstream so that the contracted flow zone was decreased.

4. Domain and Boundary Conditions

The computational domains were taken by using the western area of Koh Muang. The CAD data in STL file of DEM model is available to download on the website <http://jthatch.com/Terrain2STL/>. The data is the SRTM3 data set of the year 2000 with a resolution of about 90 meters on

the equator. The terrain surface was reconstructed by using the drape command in Rhinoceros software to make the surface with scale 1: 100, and then exported to a Parasolid file. The fluid domain was created by using the SolidWorks 3D program; that bathymetry of the river and stream was modified as a smooth channel. Next, the vicinity of the western area of Koh Muang was assumed to be a flat and high area that was given the name Original model. Then, the bypass channel was constructed in the Original model with different width sizes that

were given the names Bypass model 1, Bypass model 2, and Bypass model 3. In the junction region, the bypass channel was joined by a 90° lateral intake. The simulation modelling was performed using ANSYS Fluent commercial software. Fluid domains were extended by scaling up with 1:100.

Fig. 12 illustrates the computational domain dimension that is 1,600 m wide, 2,950 m long, and 38 m high. The Chao Phraya River flows from the southwest of the island confluence with Klong Muang canal. The highest discharges level of the Chao Phraya River is at Station C. 35, where is measured at Ban Pom, Bang Ban, Phra Nakhon Si Ayutthaya, which the maximum capacity is 1,155 m³/s and 4.58 MSL [40].

The boundary conditions that were used in the present study can be classified into four categories: mass flow inlet, pressure-inlet, pressure-outlet, and wall. The mass flow rate of Chao Phraya River is 1,153,921 kg/s of water and 1,415 kg/s of air, while the flow specification method is free surface height and bottom levels are 0.058 m and -4.522 m, respectively. The Klong Muang canal discharge was assumed by using pressure-inlet boundary condition that parameters were free surface level 0.05358 m, velocity magnitude 2.7328 m/s, and bottom level -4.521647 m, respectively. The outlet and top surfaces were considered by the pressure-outlet boundary condition. The bottom and other surface were set by a no-slip wall boundary condition. The initial

water level $h_0 = -2$ m was assumed. The water levels along Chao Phraya River were observed by different points as G1-G9.

Fig. 13(a) shows computational domain of the original model. Fig. 13(b)- Fig. 13(d) shows domain of bypass models with different width sizes of bypass channel as 46.81 m, 56.81 m, and 66.81 m for Bypass models 1, 2, and 3, respectively.

5. Computational Grid and Setup

The mesh generation strategy must be considered to accurately predict the flow near wall boundary and free-surface flow, and to reduce memory and computing effort. After trying several meshes, the mesh layer was 15 layers with first cell height = 0.25 m and growth rate 1.2. The Cartesian cut-cell grid spacing between 2.5 and 10 m was chosen as the smaller grid size applied on the river bathymetry, as seen in Fig. 14. The computational grids of each domain were 1,411,005, 1,606,880, 1,620,597, and 1,646,926, respectively. The numerical model was modelled by using the LES-VOF models. The solver type is pressure-based transient flow that includes gravitational acceleration in the y-direction of -9.81 m/s². A constant time step 0.5 s was chosen. The number of time steps was 20,000 for the flow time 1,000 s and the maximum iterations per time step was 20.

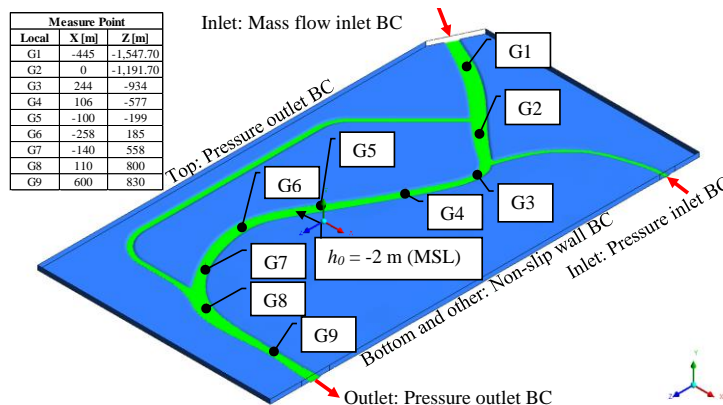


Fig. 12. Computational domain, boundary conditions and measurement point.

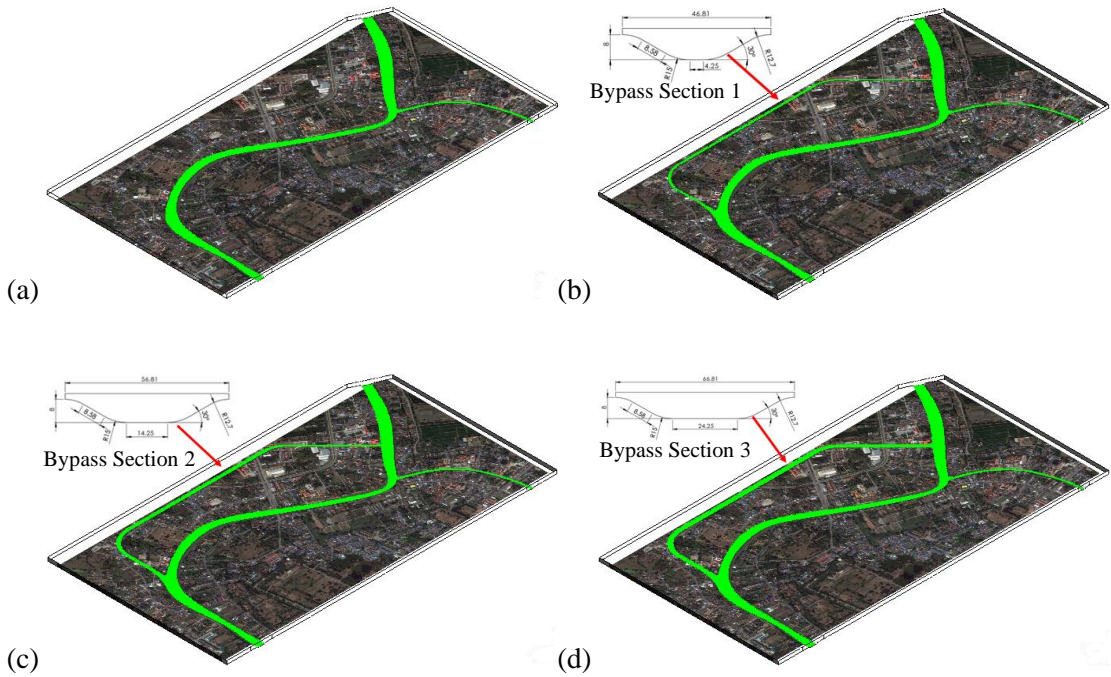


Fig. 13. Domain configurations overlay on Google Earth: (a) Original model; (b) Bypass model 1; (c) Bypass model 2; (d) Bypass model 3.

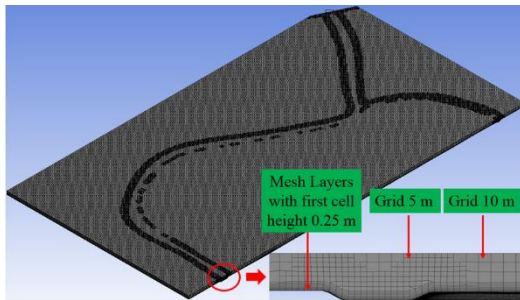


Fig. 14. Computational grid illustration of Original model.

6. Results and Discussion

The present work shows the potential application of free surface flow in 3D modelling. To investigate the effectiveness of the bypass channels, the water level and velocity pattern at flow time 1,000 s were observed. Fig. 15 shows the computed water level contour overlaid onto a Google map. The water level and river run-off in the Original model indicates a high level prior to the confluence between the Chao Phraya and

Klong Muang in the Koh Mueng area as seen in Fig. 15(a), in which the flood level contour was more than +1 m MSL. Fig. 15(b) - 15(d) show that the flood level in the Chao Phraya River decreased considerably using Bypass model 3.

Fig. 16 shows the water level from the river bed to the free-surface level at different points distributed along the center of the Chao Phraya River. The water levels were computed by using ANSYS CFD post expression language. The small planes were conducted with the perpendicular to the free-surface at any location points by using the method three points and plane bounds as rectangular with x-size = 5 m and y-size = 38 m. Then, the water level was calculated by using an area integral of volume fraction over any surfaces, and dividing by the width of the surface, for example, G1 point expression as “ $areaInt(Water.Volume\ Fraction)@Plane\ 1/(5[m])$ ”. These give water level values with the average height of the free surface at the defined planes, which results show that water

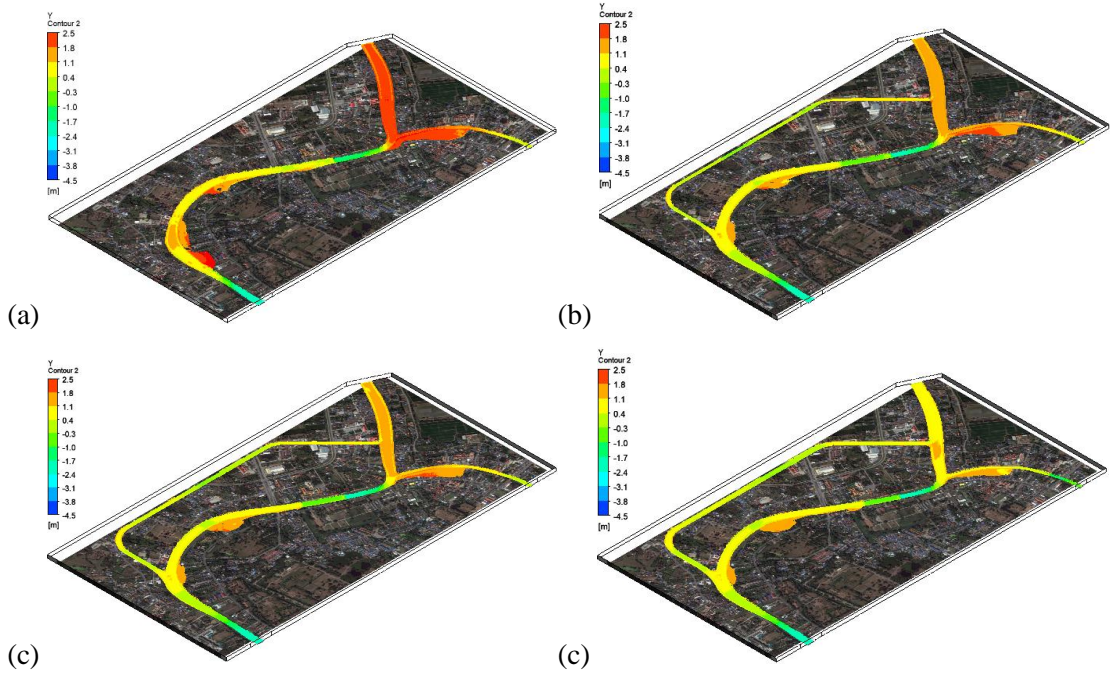


Fig. 15. Comparison results observed water level contour map in iso view at time 1,000s: a) Original, b) Bypass model 1, c) Bypass model 2 and d) Bypass model 3.

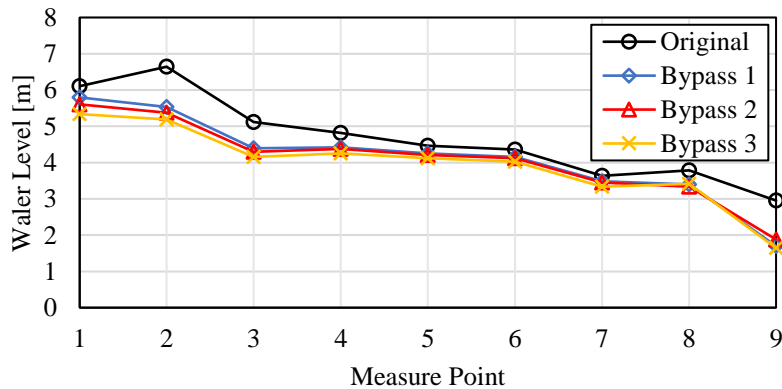


Fig. 16. Comparison results of water level at measurement points along Chao Phraya river at flow time 1,000 s.

level was decreased when using the bypass channel. The different points at G1 to G4 shows lower water level and found high level when flow passed the confluence of Chao Phraya River and Klong Muang canal. The flowing between G4 - G5 found high velocity and hydraulic jump. The hydraulic jump was formed by the rapid flowing of open channel

flow into a lower velocity zone that increased relatively suddenly the free surface flow. Moreover, the results in points G5 to G9 shows that water level was lower than in the Original model. According to 17(a), it is found that the high- and low-velocity zones in river, flood plain, and bypass junction. The high velocity on the rapidly flowing free-

surface was captured at the narrow bathymetry and slowed down when flow arrived at the channel wide river inner curve, and flooded. However, the flow velocity in the river can be decreased by applying bypass channel according to the bypass channel size, as seen in Fig. 17(b) and Fig.17(d).

Contour maps in Fig. 18(a), Fig. 18(c), and Fig. 18(e) show velocity in plain view at the bypass junction region, in which bypass channel widths were different. It is also found that the separation zone forms at the inner wall in the right-hand side in the bypass entrance region. A significant separation zone and a contracted flow zone can be observed in Bypass model 1 and Bypass model 2, but less significant was observed in the case of Bypass model 3. Furthermore, the discharge ratios (Q_r) at flow time 1,000 s of different bypass channel sizes calculated by using upstream flow divided by diversion flow that Q_r were 0.27, 0.42, and 0.53, respectively. Consequently, Bypass channel 3 diverted water discharge higher than other cases. Fig. 18(b), Fig. 18(d), and Fig. 18(f)

show that separation zones form near the bank of the confluence channel between the river and downstream bypass channel.

The velocity profiles near the free surface for different cross-sections in upstream, downstream, and bypass intake are shown in Fig. 19(a). The x- and y-axis data of Fig. 19(b)-Fig. 19(c) were normalized so that the x-axis is the width ratio of cross-section distance and the y-axis is normalized by using the maximum velocity magnitude on the free surface between G3 to G4. In this case, U_{max} is equal to 10 m/s. The upstream velocity profile compared in Fig. 19(b) to that of the Bypass model 3 shows a velocity profile higher than other cases. The downstream flow shows that the velocity profile of Bypass model 1 is maximum flow due to the least water being diverted into the bypass channel, as seen in Fig.19(c). Fig. 19(d) shows the maximum velocity profile at the contracted flow zone due to the squeeze of the separation zone that formed high velocity close to the outer bank (right hand side).

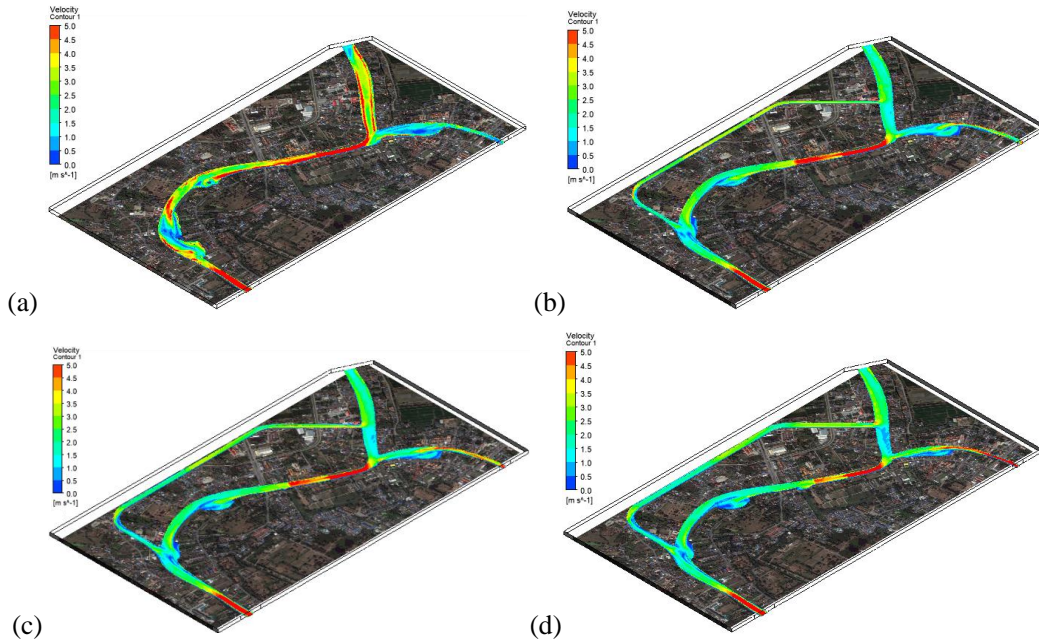


Fig. 17. Comparison results observed velocity contour in iso view at flow time 1,000 s: a) Original, b) Bypass model 1, c) Bypass model 2 and d) Bypass model 3.

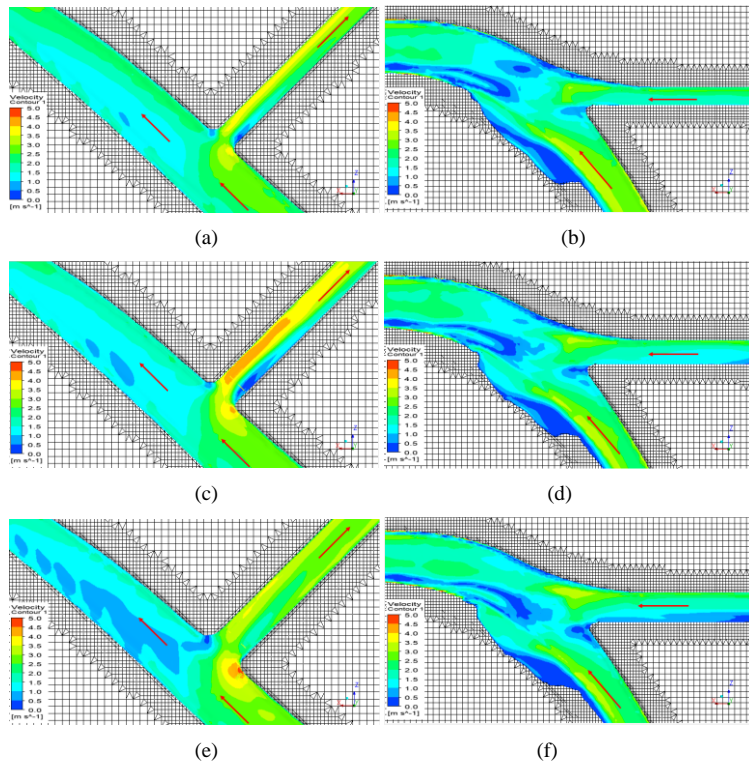


Fig. 18. Comparison results of velocity contour in plain view at the bypass channel and confluence: (a and b) Bypass model 1; (c and b) Bypass model 2; (e and f) Bypass model 3.

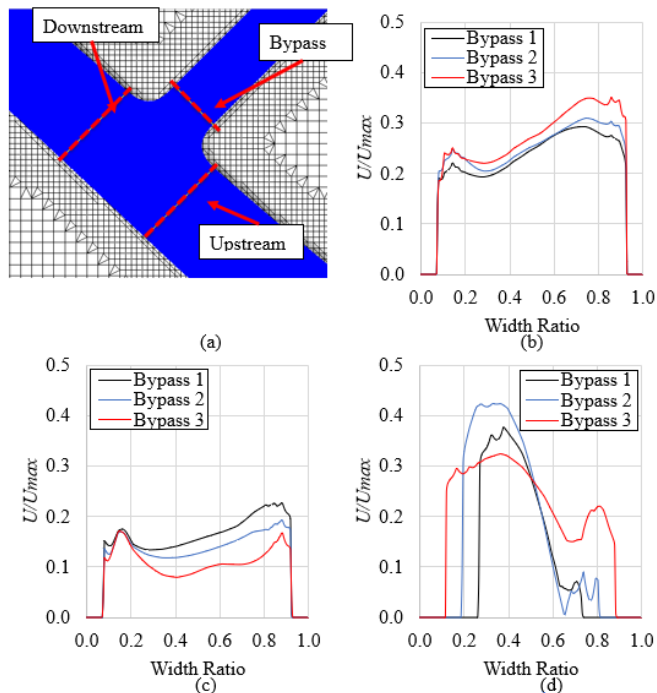


Fig. 19. Comparison results of velocity profile in plain view at the bypass intake and confluence: a) Present sections, b) Upstream profile, c) Downstream profile and d) Bypass intake profile.

6. Conclusions

The aim of the current work was to propose the 3D simulation modelling to feasibility study flood prevention by using a bypass flood diversion structure. Before applying the numerical model in the large computational domains, the different turbulence models and free surface model were validated by using experimental data of partial dam-break flow to find the proper numerical model. Then, the LES-VOF approach was chosen and applied to validate the unsteady flow of dam-break flow in channel with 90° bend model. Furthermore, flow pattern in the 90° lateral intake model (T-junction) was studied and modeled by a LES model in which meshing layers were applied.

The diversion structure in Chao Phraya River was assumed to be constructed in west land of Ayutthaya City Island, Thailand. The bypass channel was created by constructing between Wat Tha Ka Rong and Wat Chaiwatthanaram. The terrain geometry was created from the SRTM3 dataset. The free surface model was modelled based on LES-VOF models. The computational domains were generated by using the Cartesian cut-cell grid method with mesh layers and local cell refinement. The results show that the flood flow in the Chao Phraya River can be reduced by using a bypass channel with 90° lateral intake. Moreover, it is found that the formation of the separation zone in the junction region affects diversion flow; however, the length and size of the separation zone can be reduced by modifying the entrance shape.

Acknowledgment

The Thailand Research Fund (Contract No. RTA 5980009) and The Thailand Government Budget Grant provided financial support for this study.

Nomenclatures

$A_{i,j,k}$	surface area of the interface (m ²)
C_S	Smagorinsky coefficient
d	distance from the wall (m)
F_i^{vol}	volume force (N)
g	gravitational acceleration (m/s ²)
h_0	initial water depth (m)
$\kappa_{i,j,k}$	local surface curvature
l_s	mixing length for sub grid scales (m)
$n_{i,j,k}$	unit vector normal
\bar{p}	filtered pressure (Pa)
Q_r	discharge ratio
q^{th}	fluid's phase
S	rate-of-strain tensor (s ⁻¹)
\bar{S}_{ij}	rate-of-strain tensor (s ⁻¹)
Δt	time-step size (s)
U	free-stream velocity (m/s)
U_{max}	maximum velocity (m/s)
U_x	velocity of X-direction (m/s)
U_z	velocity of Z-direction (m/s)
u	velocity (m/s)
u_τ	shear velocity (m/s)
\bar{u}_i	filtered resolved quantity in the i direction (m/s)
$V_{cell,min}$	minimum volume of the computational domain (m ³)
$V_{i,j,k}$	volume of the cell (m ³)
y^+	dimensionless wall distance

Greek symbols

ρ	density (kg/m ³)
ρ_L	liquid density (kg/m ³)
μ	viscosity (Pa.s)
ν	viscosity (m ² /s)
ν_t	sub-grid eddy viscosity (m ² /s)
σ	surface tension coefficient (N/m)
α	volume fraction
τ_{ij}^r	residual stress tensor (Pa)

Abbreviations

CFL	Courant-Friedrichs-Lewy
X^*	ratio of X-direction to channel width
Z^*	ratio of Z-direction to channel width

Reference

- [1] Vojinovic Z, Keerakamolchai W, Weesakul S, Pudar R, Medina N, Alves A. Combining Ecosystem Services with Cost-Benefit Analysis for Selection of Green and Grey Infrastructure for Flood Protection in a Cultural Setting. *Environments* 2016;4:3. doi:10.3390/environments4010003.
- [2] Mah DYS, Lai SH, Aldrino R, Putuhena FJ. Investigative modelling of the flood bypass channel in Kuching, Sarawak, by assessing its impact on the inundations of Kuching-Batu Kawa-Bau Expressway. *Struct Infrastruct Eng* 2012;8: 705–14. doi:10.1080/15732471003770167.
- [3] Mah DYS, Bustami RA, Putuhena FJ. Incorporating Floodplain Inundation as a Strategy in Flood Mitigation Plan. *UNIMAS E-Journal Civ Eng* 2012;3:41-5.
- [4] Arega F, Lee JHW, Tang H. Hydraulic Jet Control for River Junction Design of Yuen Long Bypass Floodway, Hong Kong. *J Hydraul Eng* 2008;134:23–33.
- [5] Hsu, C. C., Tang, C. J., Lee, W. J., & Shieh MY. Subcritical 90° Equal-Width Open-Channel Dividing Flow. *J Hydraul Eng* 2002;128:716–20.
- [6] Lane SN, Bradbrook KF, Richards KS, Biron PA, Roy AG. The application of computational fluid dynamics to natural river channels: Three-dimensional versus two-dimensional approaches. *Geomorphology* 1999;29:1-20. doi:10.1016/S0169-555X(99)00003-3.
- [7] Neary VS, Sotiropoulos F, Odgaard a. J. Three-Dimensional Numerical Model of Lateral-Intake Inflows. *J Hydraul Eng* 1999;125:126-40. doi:10.1061/(ASCE)0733.9429(1999)125:2(126).
- [8] Barkdoll BBD, Hagen BL, Fellow AJO. Experimental Comparison of Dividing Open-Channel with Duct Flow in T-Junction. *J Hydraul Eng* 1998;124:92–5.
- [9] Rahmani Firozjaei M, Salehi Neyshabouri SAA, Amini Sola S, Mohajeri SH. Numerical Simulation on the Performance Improvement of a Lateral Intake Using Submerged Vanes. *Iran J Sci Technol - Trans Civ Eng* 2019;43: 167–77. doi: 10.1007/s40996-018-0126-z.
- [10] Shakibainia A, Tabatabai MRM, Zarrati AR. Three-dimensional numerical study of flow structure in channel confluences. *Can J Civ Eng* 2010;37:772-81. doi:10.1139/L10-016.
- [11] Larocque LA, Imran J, Chaudhry MH. 3D numerical simulation of partial breach dam-break flow using the LES and $k-\epsilon$ turbulence models. *J Hydraul Res* 2013;51:145-57. doi:10.1080/00221686.2012.734862.
- [12] Galperin B, Orszag SA. Large-eddy simulation of complex engineering and geophysical flows. Cambridge University Press; 1993.
- [13] Lv S, Gao F, Li C. Numerical simulation of 3D turbulent bend flow based on unstructured grids. *Int J Heat Technol* 2018;36:1037–46.
- [14] Kim H-J, Lee JW, Cho Y-S. Numerical Simulation of Shallow-Water Flow Using a Modified Cartesian Cut-Cell Approach. *J Eng Mech* 2010;136: 399–404. doi:10.1061/(ASCE)EM.1943-7889.0000065.
- [15] Berger M, Aftosmis M. Progress Towards a Cartesian Cut-Cell Method for Viscous Compressible Flow. 2012. doi:10.2514/6.2012-1301.
- [16] Tucker PG, Pan Z. A Cartesian cut cell method for incompressible viscous flow. *Appl Math Model* 2000;24:591–606.
- [17] Ingram DM, Causon DM, Mingham CG. Developments in Cartesian cut cell methods. *Math Comput Simul* 2003;61: 561–72. doi: 10.1016/S0378-4754(02)00107-6.

- [18] Tritthart M, Gutknecht D. Three-Dimensional Simulation of Free-Surface Flows using Polyhedral Finite Volumes. *Eng Appl Comput Fluid Mech* 2007;1:1–14. doi:10.1080/19942060.2007.11015177.
- [19] Wang X, Chen W, Zhou Z, Zhu Y, Wang C, Liu Z. Three-dimensional flood routing of a dam break based on a high-precision digital model of a dense urban area. *Nat Hazards* 2017;86: 1147– 74. doi:10.1007/s11069-016-2734-x.
- [20] Garimella R V., Shephard MS. Boundary layer meshing for viscous flows in complex domains. *7th Int Meshing Roundtable* 1998:107–118.
- [21] Hirt CW, Sicilian JM. A Porosity Technique for the Definition of Obstacles in Rectangular Cell Meshes. (*Flow Sci Inc*) 1985:450–68.
- [22] Rostami F, Rezaei-manizani H, Mastorakis NE. Comparison of the Results of 2D and 3D Numerical Modeling of Flow over Spillway Chutes with Vertical Curvatures. *Int J* 2007;1.
- [23] Janßen CF, Grilli ST, Krafczyk M. On enhanced non-linear free surface flow simulations with a hybrid LBM-VOF model. *Comput Math with Appl* 2013;65: 211– 29. doi:10.1016/j.camwa.2012.05.012.
- [24] Kajzer, A., Pozorski, J., and Szevc K. Large-eddy simulations of 3D Taylor-Green vortex: comparison of Smoothed Particle Hydrodynamics, Lattice Boltzmann and Finite Volume methods. *XXI Fluid Mech. Conf.*, vol. 530, 2014. doi:10.1088/1742-6596/530/1/012019.
- [25] Kao H- M, Chang T- J. Numerical modeling of dambreak-induced flood and inundation using smoothed particle hydrodynamics. *J Hydrol* 2012;448–449: 232– 44. doi:10.1016/j.jhydrol.2012.05.004.
- [26] Biscarini C, Francesco SD, Nardi F, Manciola P. Detailed Simulation of Complex Hydraulic Problems with Macroscopic and Mesoscopic Mathematical Methods. *Math Probl Eng* 2013;2013.
- [27] Albano R, Sole A, Mirauda D, Adamowski J. Modelling large floating bodies in urban area flash-floods via a Smoothed Particle Hydrodynamics model. *J Hydrol* 2016;541: 344– 58. doi:10.1016/j.jhydrol.2016.02.009.
- [28] Marsooli R, Wu W. 3-D finite-volume model of dam-break flow over uneven beds based on VOF method. *Adv Water Resour* 2014;70: 104– 17. doi:10.1016/j.advwatres.2014.04.020.
- [29] Hirt CW, Nichols BD. Volume of fluid (VOF) method for the dynamics of free boundaries. *J Comput Phys* 1981;39: 201– 25. doi: 10. 1016/ 0021-9991(81)90145-5.
- [30] Ubbink O, Issa RI. A Method for Capturing Sharp Fluid Interfaces on Arbitrary Meshes. *J Comput Phys* 1999;50:26–50.
- [31] Ubbink O. Numerical prediction of two fluid systems with sharp interfaces. *Splash* 1997:69. doi:10.1145/1774088.1774119.
- [32] Munoz DH, Constantinescu G. Advances in Water Resources A fully 3- D numerical model to predict flood wave propagation and assess efficiency of flood protection measures. *Adv Water Resour* 2018;122: 148– 65. doi:10.1016/j.advwatres.2018.10.014.
- [33] Malvin A, Chan A, Lau PL. Large eddy simulation of distillation sieve tray hydrodynamics - A volume-of-fluid (VOF) Approach. *Eng Lett* 2011;19.
- [34] Smagorinsky J. General Circulation Experiments With the Primitive Equations. *Mon Weather Rev* 1963;91:99–164.

- [35] Brackbill JU, Kothe DB, Zemach C. A continuum method for modeling surface tension. *J Comput Phys* 1992;100:335–54.
- [36] Nadooshan AA, Shirani E. Numerical Simulation of a Single Air Bubble Rising in Water with Various Models of Surface Tension Force. *World Acad Sci Eng Technol* 2008;39:72–6.
- [37] Bayon A, Valero D, García-bartual R, Jos F. Environmental Modelling & Software Performance assessment of OpenFOAM and FLOW- 3D in the numerical modeling of a low Reynolds number hydraulic jump Vall e. *Environ Model Softw J* 2016;80: 322– 35. doi:10.1016/j.envsoft.2016.02.018.
- [38] Frazão SS, Zech Y. Effects of a Sharp Bend on Dam-Break Flow. *Proc. , 28th IAHR Congr.*, 1999, p. CD-ROM.
- [39] Goudarzizadeh R, Hedayat N, Jahromi SHM. Three-dimensional Simulation of Flow Pattern at the Lateral Intake in Straight Path , using Finite- Volume Method. *World Acad Sci Eng Technol* 2010;4:656–61.
- [40] Royal Irrigation. Chao Phraya River water situation report. Internet n. d. http://www.hydro-5.com/index_.php?id=100P (accessed March 20, 2017).